JCTC Journal of Chemical Theory and Computation

Article

pubs.acs.org/JCTC

# Self-Modulated Band Structure Engineering in $C_4F$ Nanosheets: First-Principles Insights

Yafei Li,*[,†] Bay Allen Pantoja,[‡] and Zhongfang Chen*[,‡]

[†]College of Chemistry and Materials Science, Jiangsu Key Laboratory of Biofunctional Materials, Nanjing Normal University, Nanjing, Jingsu, 210046, China

[‡]Department of Chemistry, Institute for Functional Nanomaterials, University of Puerto Rico, Rio Piedras Campus, San Juan, Puerto Rico 00931

Supporting Information

**ABSTRACT:** Density functional theory (DFT) computations with van der Waals (vdw) correction revealed the existence of considerable $C^{\delta+}F^{\delta-}\cdots C^{\delta+}F^{\delta-}$ dipole−dipole interactions between two experimentally realized $C_4F$ monolayers. The dipole−dipole interactions induce a subtle interlayer polarization, which results in a significantly reduced band gap for $C_4F$ bilayer as compared to the individual $C_4F$ monolayer. With increasing the number of stacked layers, the band gap of $C_4F$ nanosheets can be further reduced, leading to a semiconducting−metallic transition. Moreover, the band gap of $C_4F$ nanosheets can be feasibly modulated by applying an external electric field. Our results provide new insights on taking advantage of nonbonding interactions to tune the electronic properties of graphene materials.

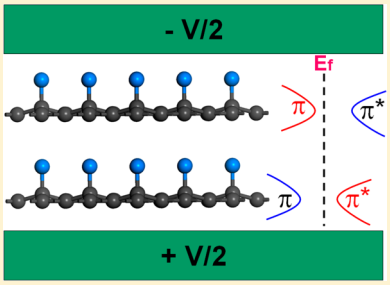


## INTRODUCTION

Graphene,[1] the first experimentally identified two-dimensional (2D) crystal, has fascinating properties, including massless Dirac fermions,[2] ultrahigh carrier mobility,[3] exceptional mechanic strength,[4]and superior thermal conductivity.[5] These properties enable graphene to be very attractive for various applications, such as lithium ion batteries (LIBs),[6] electrochemical capacitors,[7] biosensors,[8] and solar cells.[9] It is even believed that graphene can replace the role of traditional silicon materials in microelectronics in the very near future.[10] However, it is well-known that pristine graphene is semimetallic, and the lack of a suitable band gap is a limiting factor for us to utilize graphene in many important fields, such as the channel material for field-effect transistors, which reply on the principal band gap to switch on/off the electric current. Therefore, a band gap must be opened before any "graphenium" microprocessor can be realized.[11,12]

The simplest way to achieve this target is cutting 2D graphene into one-dimensional graphene nanoribbons (GNRs), which have a nonzero band gap independent of their edge orientation (zigzag or armchair) or width.[13−16] However, at present, it is still difficult to scale up the production of GNRs with well-defined edges as well as assemble them into functional devices. Applying uniaxial strain[17] or external electric field[18,19] can also open a gap in the band structure of graphene, but the values of opened band gap are too tiny (<0.3 eV) for practical applications, mostly due to the robust $\pi$-bands of graphene.

Chemical functionalization is able to open a band gap for graphene,[20] and an efficient method is converting its carbon atoms from $sp^2$ to $sp^3$ hybridization through hydrogenation or fluorination. Both experimental and theoretical studies demonstrated that a considerable band gap can be opened in fully hydrogenated (graphane)[21−25] or fluorinated (fluorographene)[26−28] graphene. However, the band gaps of graphane and fluorographene are too large (>3.0 eV) for practical applications, especially in electronics and optoelectronics.

Interestingly, by means of van der Waals (vdW) corrected density functional theory (DFT) computations, we demonstrated recently that there exists considerable C−H···F−C bonding between graphane and fluorographene layers,[29] and the assembled graphane/fluorographene bilayer has a band gap much lower than those of individual graphane and fluorographene monolayers, which opens a new route for band gap engineering of graphene materials.

Recently, several groups successfully synthesize a new 2D graphene fluoride, in which the F/C ratio is 1:4.[30−32] In the $C_4F$ monolayer, F atoms are all adsorbed on one side and arranged in a *para*-type chemisorption pattern, leaving all of the $sp^2$ carbon atoms in benzenoid rings. Theoretical studies demonstrated that the $C_4F$ monolayer also has a wide band gap of ∼3.0 eV.[33−36] Because of the large difference in electronegativity, F atoms and F-bonded $sp^3$ C atoms in the $C_4F$ monolayer would be charged oppositely. As a result, the electrostatic interactions between permanent dipoles in the bilayer system could lead to considerable $C^{\delta+}F^{\delta-}\cdots C^{\delta+}F^{\delta-}$ dipole−dipole interactions in addition to the normal vdW interaction at the interface of $C_4F$ nanosheets. Motivated by the recent extensive studies of using weak interactions to tune the electronic properties of 2D materials,[29,37−42] we are more

Received: December 16, 2013
Published: January 23, 2014

   dx.doi.org/10.1021/ct401083c | J. Chem. Theory Comput. 2014, 10, 1265−1271

interested in how the potential dipole−dipole interactions would modify the electronic properties of $C_4F$ nanosheets.

To address this issue, we have performed vdW corrected DFT computations. For the first time, we revealed there exist considerable $C^{\delta+}F^{\delta-}\cdots C^{\delta+}F^{\delta-}$ dipole−dipole interactions between the $C_4F$ bilayer. The dipole−dipole interaction not only defines the stacking pattern of the $C_4F$ layer, but also endows it a remarkably reduced band gap as compared to that of the $C_4F$ monolayer. Additionally, we demonstrated that the band gap of $C_4F$ nanosheets can be flexibly tuned by applying an external electric field. Our results would provide new ideas to tune the electronic properties of graphene materials toward novel electronic and optical devices.

## COMPUTATIONAL DETAILS

DFT computations based on first-principles were performed using the plane-wave technique implemented in Vienna ab initio simulation package (VASP).[43] The ion−electron interaction was described using the projector-augmented plane wave (PAW) approach.[44] The generalized gradient approximation (GGA) expressed by the PBE functional[45] and a 420 eV cutoff for the plane-wave basis set were adopted in all computations. Earlier studies demonstrated that the PBE functional can well predict the geometric structures for graphite fluorides.[46] However, it is known that weak interactions are out of the framework of the standard PBE functional; thus we adopted the PBE+D2 (D stands for dispersion) method with the Grimme vdW correction[47] to describe the weak interactions. The accuracy of PBE+D2 has been well validated in recent literature.[29,48]

We set the $x$ and $y$ directions parallel and the $z$ direction perpendicular to the $C_4F$ plane, and adopted a supercell length of 25 Å in the $z$ direction. The geometry optimizations were performed by using the conjugated gradient method, and the convergence threshold was set to be $10^{-4}$ eV in energy and $10^{-3}$ eV/Å in force. The Brillouin zone was represented by a Monkhorst−Pack special $k$-point mesh of 6 × 6 × 1 for geometry optimizations, while a larger grid (20 × 20 × 1) was used for band structure computations.

The binding energy of $C_4F$ bilayer ($E_b$) is defined as: $E_b = (2E_{monolayer} - E_{bilayer})/2$, where $E_{bilayer}$ and $E_{monolayer}$ are the total energies of $C_4F$ bilayer and monolayer, respectively. According to this definition, the bilayer structures with higher $E_b$ are more stable.

## RESULTS AND DISCUSSION

**Structural and Electronic Properties of 2D $C_4F$ Monolayer.** First, we have studied the structure and electronic properties of the $C_4F$ monolayer. Figure 1a presents the optimized geometric structure of the $C_4F$ monolayer in a 3 × 3 supercell. One unit cell of $C_4F$ monolayer consists of 8 carbon atoms and two fluorine atoms with the lattice parameters optimized to be $a = b = 4.96$ Å. Therefore, the unit cell of $C_4F$ monolayer is about 4 times that of graphene.

In the $C_4F$ monolayer, 25% carbon atoms transform from $sp^2$ to $sp^3$ hybridization due to the fluorination, while the rest of the $sp^2$ carbon atoms ($C_{sp2}$) are all in benzenoid rings, which are separated from each other by F atoms. Therefore, the stability of $C_4F$ monolayer is essentially enhanced by the aromatic stabilization,[49] which also has been revealed in the $BC_3$ monolayer.[50] Note that the $C_4F$ monolayer is not perfectly planar, and the planes of $sp^2$ and $sp^3$ carbon atoms ($C_{sp3}$) are

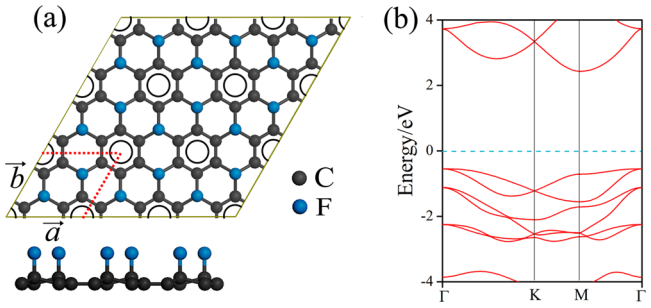


**Figure 1.** (a) Top (upper) and side (bottom) views of geometric structure of 2D $C_4F$ monolayer. The red dashed lines indicate a unit cell. The black circles represent the benzenoid rings. (b) Band structure of $C_4F$ monolayer computed using PBE functional. The green dashed line denotes the position of the Fermi level.

separated by a height of 0.35 Å. The lengths of $C_{sp3}-C_{sp2}$, $C_{sp2}-C_{sp2}$, and $C_{sp3}-F$ bonds are 1.51, 1.40, and 1.45 Å, respectively. Because of the large electronegativity difference between C and F, the $C_{sp3}-F$ bonds in the $C_4F$ monolayer are partially ionic rather than perfect covalent. According to the Bader charge population analysis, $C_{sp3}$ and F atoms possess a 0.6 |e| positive and negative charge, respectively. Moreover, $C_4F$ monolayer is semiconducting with a 2.98 eV indirect energy gap at the PBE level of theory, with the valence band maximum (VBM) and conduction band minimum (CBM) located at the Γ and M points, respectively (Figure 1b). Our results agree well with previous studies.[33−36]

**Structural and Electronic Properties of the $C_4F$ Bilayer.** The $C_4F$ bilayer can be easily constructed by stacking two $C_4F$ monolayers together. Considering the structural properties of the $C_4F$ monolayer, the $C_4F$ bilayer may have three possible stacking patterns: (I) C plane versus F plane, (II) F plane versus F plane, and (III) C plane versus C plane. For each stacking pattern, we performed a set of lateral shifts of one $C_4F$ monolayer to the basal plane of the other and obtained several stable configurations (see the Supporting Information). The energetically most favorable configurations for each stacking pattern are presented in Figure 2.

In the lowest-energy configuration of $C_4F$ bilayer in pattern I (Figure 2), the F atoms of the bottom $C_4F$ monolayer point straight to the $C_{sp3}$ atoms of the upper layer with an interlayer

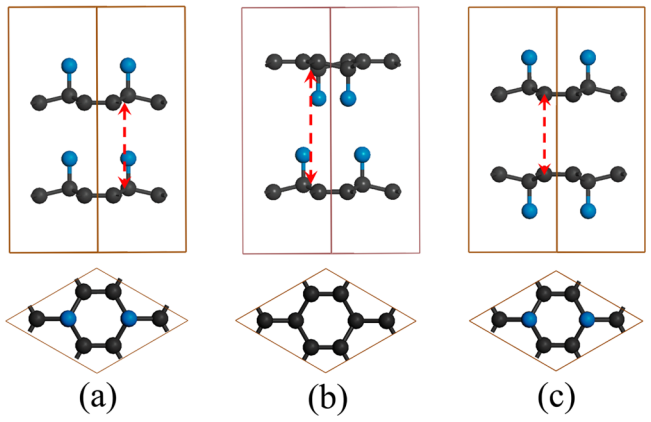


**Figure 2.** Side (upper) and top (bottom) views of the energetically most stable configurations of $C_4F$ bilayer in three different stacking patterns. The red double-headed arrow denotes the distance between two carbon skeletons.


dx.doi.org/10.1021/ct401083c | J. Chem. Theory Comput. 2014, 10, 1265−1271

$C_{sp3}$–F distance of 3.09 Å. The $E_b$ of this configuration is 231 meV per unit cell. For comparison, the $E_b$ values of graphene bilayer and graphane bilayer in a 2 × 2 supercell are 528 and 256 meV, respectively. Therefore, the interlayer coupling of $C_4F$ bilayer is weaker than that of the graphene bilayer but comparable to that of the graphane bilayer.

The long distance between two carbon skeletons (4.54 Å) in $C_4F$ bilayer precludes the $p_\pi$–$p_\pi$ interaction, which dominates in the graphene bilayer. The interlayer forces between $C_4F$ layers should be mainly contributed by the attractive $C^{\delta+}F^{\delta-}\cdots C^{\delta+}F^{\delta-}$ dipole–dipole interactions. Note that F atoms and the plane of $C_{sp2}$ atoms have a distance of 2.74 Å; thus subtle anion–$\pi$ interactions between two $C_4F$ layers could also exist.

Moreover, the $C^{\delta+}F^{\delta-}\cdots C^{\delta+}F^{\delta-}$ dipole–dipole interactions also induce an interesting spontaneous interlayer polarization with a 0.02 e/unit cell charge transfer from the upper $C_4F$ layer to the bottom layer, which would not only contribute to the stabilization of the bilayer but also modify the electronic properties correspondingly.

In the most stable configuration of $C_4F$ bilayer in pattern II, the two carbon skeletons are in AA stacking, and the F atoms of each monolayer point to the $C_{sp2}$ atoms of the other monolayer. To minimize the repulsive $F^{\delta-}\cdots F^{\delta-}$ interactions, the two $C_{sp3}$ skeletons are separated by a large distance of 5.24 Å (Figure 2), and the distance between two F atom planes is 2.76 Å; this separation results in a rather small $E_b$ of 44 meV/unit cell. In contrast to the $C_4F$ bilayer in pattern I, there is only negligible interlayer charge transfer (0.001 e/unit cell) for the $C_4F$ bilayer in pattern II.

The most stable configuration of the $C_4F$ bilayer in pattern III also has the two carbon skeletons in AA stacking and the benzenoid rings of each $C_4F$ monolayer pointing directly to those of the other monolayer. Although there could exist subtle $\pi$–$\pi$ interactions between benzenoid rings, the two carbon skeletons are still separated by a distance of 4.24 Å to minimize the repulsive $C^{\delta+}\cdots C^{\delta+}$ interactions. There is only a slight interlayer polarization and 0.004 e/unit cell charge transfers from the bottom $C_4F$ layer to the upper $C_4F$ layer, which would help to stabilize the bilayer structure. As a result, the $C_4F$ bilayer in pattern III has a more favorable $E_b$ (135 meV/unit cell) than that in pattern II.

Overall, due to the lack of attractive $C^{\delta+}F^{\delta-}\cdots C^{\delta+}F^{\delta-}$ dipole–dipole interactions, the $E_b$ values of configurations in patterns II and III are both much lower than that of pattern I. Therefore, when obtained experimentally, the $C_4F$ bilayer as well as thicker nanosheets should be stacked mostly via pattern I. In the following parts, we refer to the most stable configuration of the $C_4F$ bilayer in pattern I as the $C_4F$ bilayer unless stated otherwise.

Our above computations demonstrate that considerable interlayer coupling exists between two $C_4F$ layers if they are stacked in the right pattern. How does this kind of interlayer coupling affect the electronic properties? To this end, we computed the band structure of the $C_4F$ bilayer.

As shown in Figure 3a, surprisingly, the $C_4F$ bilayer has a significantly reduced indirect band gap of 0.86 eV, much smaller than that of the $C_4F$ monolayer (2.98 eV). Same as the $C_4F$ monolayer, the VBM and CBM of $C_4F$ bilayer are also located at the M and Γ points, respectively. Especially, the $C_4F$ bilayer has a direct gap of 1.06 eV at the M point, suggesting very promising applications in optoelectronics.

Moreover, considering that standard GGA usually underestimates band gaps of semiconducting materials, we also

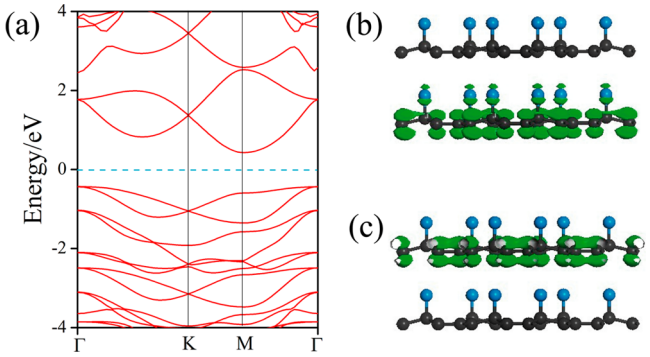


**Figure 3.** (a) Band structure of the $C_4F$ bilayer computed using the PBE functional. (b and c) Partial charge densities of (b) CBM and (c) VBM of the $C_4F$ bilayer.

computed the band gaps of $C_4F$ bilayer as well as monolayer by using the newly developed HSE06 hybrid functional[51,52] for validation (see the Supporting Information). The HSE06 band gaps for the $C_4F$ monolayer and bilayer are 4.03 and 1.83 eV, respectively, indicating that HSE06 and PBE actually predict qualitatively the same trends.

We have also computed the band structures of the metastable configurations of $C_4F$ bilayer in pattern I (see the Supporting Information). Interestingly, these metastable configurations have quite close band gaps as the most stable one, indicating that the band gap reduction in $C_4F$ bilayer is rather robust against the variation in interface alignments.

Therefore, our computations reveal that the interlayer coupling between two $C_4F$ layers leads to a fascinating self-modulated band gap reduction. The similar behavior has been demonstrated in hydrogenated BN nanosheets due to the formation of interlayer dihydrogen bonds,[41,42] but it is the first time that such an interesting phenomenon has been revealed in graphene materials.

To give a better interpretation of the band gap reduction in $C_4F$ bilayer, we computed the partial charge densities corresponding to the VBM and CBM of the $C_4F$ bilayer (Figure 3b and c). We found that the VBM and CBM of $C_4F$ bilayer are localized on the upper and bottom layers, respectively. The VBM is contributed solely by the benzenoid rings of the upper $C_4F$ monolayer, while the CBM is contributed by the fluorine atoms and $C_{sp2}$ atoms of the bottom $C_4F$ monolayer.

What is the driving force for the recombination of energy levels? As mentioned above, the $C^{\delta+}F^{\delta-}\cdots C^{\delta+}F^{\delta-}$ dipole–dipole interactions induce a spontaneous interlayer polarization in the $C_4F$ bilayer featured by charge transfer from the upper $C_4F$ layer to the bottom layer. To understand the effect of interlayer polarization, we plotted the plane-averaged electrostatic potential along the normal of the $C_4F$ bilayer. As shown in Figure 4, a considerable electrostatic potential difference around the 2D interface can be clearly identified; the electrostatic potential of the upper $C_4F$ layer is significantly raised relative to that of the bottom $C_4F$ layer. Consequently, the energy levels of the upper $C_4F$ layer are shifted upward relative to those of the bottom layer, leading to a staggered band lineup and a decrease in the band gap. Therefore, our analysis revealed that it is the $C^{\delta+}F^{\delta-}\cdots C^{\delta+}F^{\delta-}$ dipole–dipole interaction (due to the electrostatic interactions between the permanent dipoles in the two $C_4F$ layers)-induced spontaneous


dx.doi.org/10.1021/ct401083c | J. Chem. Theory Comput. 2014, 10, 1265–1271

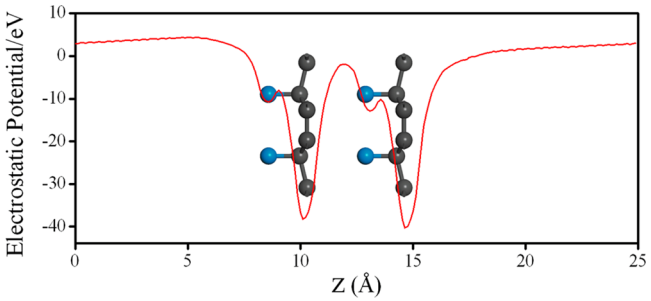


**Figure 4.** Plane-averaged electrostatic potential along the $C_4F$ bilayer normal.

interlayer polarization that accounts for the significant band gap reduction in the $C_4F$ bilayer.

To further validate our assumption, we also computed the band structures of the most stable configuration $C_4F$ bilayer in patterns II and III (see the Supporting Information), in which $C^{\delta+}F^{\delta-}\cdots C^{\delta+}F^{\delta-}$ dipole−dipole interactions are absent and the interlayer polarizations are weaker. According to our computations, the $C_4F$ bilayer in pattern II has a band gap of 2.88 eV, which is quite close to that of the $C_4F$ monolayer due to the negligible interlayer polarization. Interestingly, the $C_4F$ bilayer in pattern III has a slightly reduced band gap of 2.59 eV as compared to the $C_4F$ monolayer, which also can be attributed to the appreciable (but still much smaller than that in pattern I) interlayer polarization.

**Structural and Electronic Properties of $C_4F$ Multilayers.** After knowing that band gap can be significantly reduced in $C_4F$ bilayer, it is natural for us to explore whether the band gap can be further reduced by increasing the stacked layers. Therefore, we have investigated the electronic properties of $C_4F$ nanosheets with the layer number up to 5.

For these $(C_4F)_n$ ($n$ = 3, 4, 5) nanosheets, the structural properties are similar to these of the $C_4F$ bilayer: in the energetically preferred structures, the carbon skeletons are in AA stacking, and F atoms of the bottom layer point to the $C_{sp3}$ atoms of the upper layer.

The band gap of $C_4F$ nanosheets as a function of layer number is presented in Figure 5a. Apparently, the band gap of $C_4F$ nanosheets decreases rapidly with increasing the number of layers. Especially, when $n$ reaches to 4, the band gap becomes zero, indicating that $C_4F$ nanosheets are metallic at this thickness.

To get a deep understanding, we computed the partial charge densities corresponding to VBM and CBM of $(C_4F)_3$ and $(C_4F)_4$ nanosheets. Similar to the $C_4F$ bilayer, the localization of VBM and CBM was also found in $(C_4F)_3$ and $(C_4F)_4$ nanosheets. With increasing thickness, the CBM moves continuously to the newly attached layer (Figure 5b,c), resulting in a further decrease in the band gap and finally a semiconducting−metallic transition.

**The Effect of External Electric Field.** Recently, many studies demonstrated that the electronic properties of 2D materials can be significantly modified by applying an external electric field (E-field).[29,41,42,53,54] For example, our theoretical study revealed that the E-field can cause a fantastic semiconducting−metallic transition in the graphane/fluorographene bilayer, depending on the strength and direction of the field.[29] Considering that controllable band gap engineering is always experimentally meaningful, we systematically examined the effect of the E-field on the electronic properties of $C_4F$ layers by

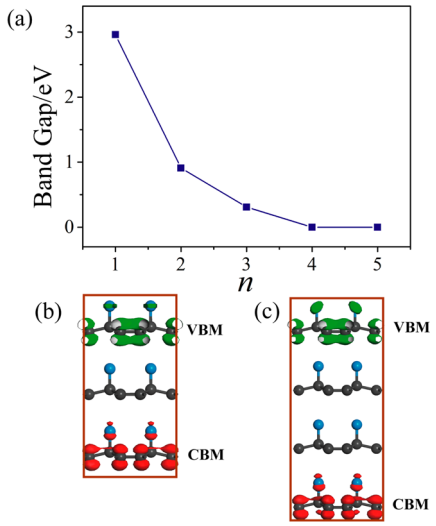


**Figure 5.** (a) Band gaps of $(C_4F)_n$ as a function of the number of layers $n$ computed using the PBE functional. (b and c) The partial charge densities of VBM (green) and CBM (red) for $(C_4F)_3$ and $(C_4F)_4$.

choosing $C_4F$ bilayer as a representative. Two directions of the E-field ($+z$, $-z$) vertical to the basal plane of $C_4F$ layers were considered, and we defined the positive direction of the E-field as pointing from the bottom $C_4F$ layer to the upper $C_4F$ layer (Figure 6a). The band gap of $C_4F$ bilayer as a function of the magnitude of the E-field is plotted in Figure 6b.

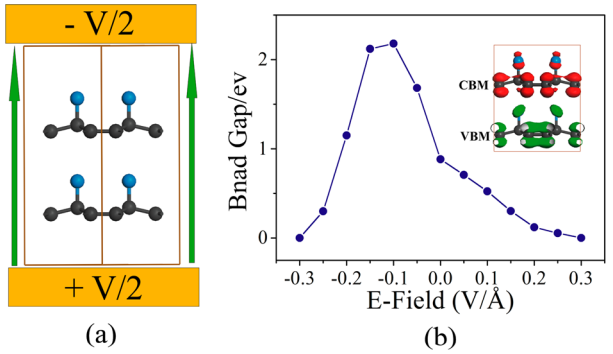


**Figure 6.** (a) Schematic diagram of $C_4F$ bilayer with the E-field. The arrows denote the positive direction of the field. (b) Band gap of $C_4F$ bilayer as a function of E-field computed using the PBE functional. The inserted figure shows the partial charge densities of VBM and CBM of the $C_4F$ bilayer at the E-field of −0.2 V/Å.

As a comparison, we also explored the effect of the E-field on the electronic properties of $C_4F$ monolayer. However, it was found the band gap of $C_4F$ monolayer is rather robust to the E-field.

In stark contrast, our computations revealed that the electronic properties of $C_4F$ bilayer are rather sensitive to the E-field. With a positive E-field, the band gap decreases gradually with increasing the E-field strength (Figure 6b). When the E-field reaches 0.3 V/Å, the $C_4F$ bilayer tunes to be metallic. In contrast, when the E-field is applied in the negative direction, the band gap first increases as the E-field strength increases. Interestingly, when the E-field reaches −0.15 V/Å, the band gap decreases rapidly with increasing E-field strength, and can also become zero at −0.3 V/Å.


dx.doi.org/10.1021/ct401083c | J. Chem. Theory Comput. 2014, 10, 1265−1271

The E-field-induced semiconducting−metallic transition in $C_4F$ bilayer essentially originates from the opposite effect of the E-field on VBM and CBM, which are localized at the upper and bottom $C_4F$ monolayer, respectively. With a positive E-field, the electrostatic potential on the upper $C_4F$ monolayer is lifted, while that on the bottom $C_4F$ monolayer is lowered. Correspondingly, the VBM on the upper $C_4F$ layer is further shifted upward, while the CBM on the bottom $C_4F$ moves downward; thus the band gap decreases as the E-field increases, eventually converting $C_4F$ bilayer into metallic. In contrast, with a negative E-field, the electrostatic potential is lowered on the upper $C_4F$ layer and raised on the bottom $C_4F$ layer. Therefore, the energy levels of the upper $C_4F$ are shifted downward and those on the bottom layer upward, leading to an increase of band gap. It is expected that the $C_4F$ bilayer can have the same band gap as the $C_4F$ monolayer at a critical value of E-field. Once the strength of negative E-field exceeds this critical value, the localization of VBM and CBM can happen again. Yet at this time, the VBM is localized at the bottom $C_4F$ layer while the CBM is localized at the upper $C_4F$ layer (Figure 6b). As the strength of negative E-field increases, the energy levels of bottom $C_4F$ layer would be shifted upward while those of the bottom layer downward, leading to a decrease of the band gap. Note that the critical E-field required for semiconducting−metallic transition (0.3 V/Å) is experimentally realizable.[55,56] Therefore, it is rather flexible to tune the electronic properties of $C_4F$ bilayer by applying an external field.

## CONCLUSION

To summarize, by means of vdW corrected DFT computations, we systemically studied the structural and electronic properties of $C_4F$ nanosheets. It is found that the lowest-energy configuration of $C_4F$ bilayer is in the isotropic stacking pattern and featured with considerable $C^{\delta+}F^{\delta-}\cdots C^{\delta+}F^{\delta-}$ dipole−dipole interactions between two layers. Especially, the dipole−dipole interactions between $C_4F$ layers induce a subtle interlayer polarization, which significantly reduces the band gap of $C_4F$ monolayer and coverts it from insulating to semiconducting. The band gap can be further reduced to zero by increasing the number of $C_4F$ layers. Interestingly, the electronic properties of $C_4F$ bilayer are quite sensitive to the external E-field. A semiconductor−metal transition can be achieved by applying an external E-field, independent of the direction of E-field. Our studies suggest a rather flexible way toward tuning the electronic properties of graphene derivatives and provide new insights for designing weak interactions dominated nanomaterials with promising technological applications. Considering the recent progress on the self-assembly of graphene materials,[57] we believe that the stacked $C_4F$ nanosheets with self-reduced band gaps can be realized experimentally soon. We also hope that the similar self-modulated gap-reduction mechanism can be found in other graphene materials, such as $C_4H$[58,59] and $C_4Cl$,[60] which are structural analogues of $C_4F$ and have been realized experimentally.

## ASSOCIATED CONTENT

### Supporting Information

All of the stable configurations of $C_4F$ bilayer in three stacking patterns, band structures of $C_4F$ bilayer and monolayer computed using HSE06 hybrid functional, band structures of metastable configurations of $C_4F$ bilayer in pattern I, and band structures of the most stable configurations $C_4H$ bilayer in patterns II and III. This material is available free of charge via the Internet at http://pubs.acs.org.

## AUTHOR INFORMATION

### Corresponding Authors

*E-mail: liyafei.abc@gmail.com.
*E-mail: zhongfangchen@gmail.com.

### Notes

The authors declare no competing financial interest.

## ACKNOWLEDGMENTS

Support in China by startup funds of Nanjing Normal University (184080H20145) and in the U.S. by the Department of Defense (Grant W911NF-12-1-0083) is gratefully acknowledged.

## REFERENCES

(1) (a) Novoselov, K. S.; Geim, A. K.; Morozov, S. V.; Jiang, D.; Zhang, Y.; Dubonos, S. V.; Gregorieva, I. V.; Firsov, A. A. Electric Field Effect in Atomically Thin Carbon Films. *Science* **2004**, *306*, 666−669. (b) Novoselov, K. S.; Jiang, D.; Schedin, F.; Booth, T. J.; Khotkevich, V. V.; Morozov, S. V.; Geim, A. K. Two-Dimensional Atomic Crystals. *Proc. Natl. Acad. Sci. U.S.A.* **2005**, *102*, 10451−10453.

(2) Novoselov, K. S.; Geim, A. K.; Morozov, S. V.; Jiang, D.; Khotkevich, I. V.; Gregorieva, I. V.; Dubonos, S. V.; Firsov, A. A. Two-Dimensional Gas of Massless Dirac Fermions in Graphene. *Nature* **2005**, *438*, 197−200.

(3) Morozov, S. V.; Novoselov, K. S.; Katsnelson, M. I.; Schedin, F.; Elias, D.; Jaszczak, J. A.; Geim, A. K. Giant Intrinsic Carrier Mobilities in Graphene and Its Bilayer. *Phys. Rev. Lett.* **2008**, *100*, 016602.

(4) Lee, C. G.; Wei, X. D.; Kysar, J. W.; Hone, J. Measurement of the Elastic Properties and Intrinsic Strength of Monolayer Graphene. *Science* **2008**, *321*, 385−388.

(5) Balandin, A. A.; Ghosh, S.; Bao, W.; Calizo, I.; Teweldebrhan, D.; Miao, F.; Lau, C. N. Superior Thermal Conductivity of Single-Layer Graphene. *Nano Lett.* **2008**, *8*, 902−907.

(6) Yoo, E. J.; Kim, J.; Hosono, E.; Zhou, H. S.; Kudo, T.; Honma, I. Large Reversible Li Storage of Graphene Nanosheet Families for Use in Rechargeable Lithium Ion Batteries. *Nano Lett.* **2008**, *8*, 2277−2282.

(7) Stoller, M. D.; Park, S.; Zhu, Y.; An, J.; Ruoff, R. S. Graphene-Based Ultracapacitors. *Nano Lett.* **2008**, *8*, 3498−3502.

(8) (a) Garaj, W.; Hubbard, W.; Reina, A.; Kong, J.; Branton, D.; Golovchenko, J. A. Graphene as a subnanometre trans-electrode membrane. *Nature* **2010**, *467*, 190−194. (b) Merchant, C. A.; Healy, K.; Wanunu, M.; Ray, V.; Peterman, N.; Bartel, J.; Fischbein, M. D.; Venta, K.; Luo, Z.; Johnson, A. T. C.; Drndić, M. DNA Translocation Through Graphene Nanopores. *Nano Lett.* **2010**, *10*, 2915−2921. (c) Schneider, G. F.; Kowalczyk, S. W.; Calado, V. E.; Pandraud, G.; Zandbergen, H. W.; Vandersypen, L. M. K.; Dekker, C. DNA Translocation Through Graphene Nanopores. *Nano Lett.* **2010**, *10*, 3163−3167.

(9) Wang, X.; Zhi, L.; Müllen, K. Transparent, Conductive Graphene Electrodes for Dye-Sensitized Solar Cells. *Nano Lett.* **2008**, *8*, 323−327.

(10) Lemme, M. C.; Echtermeyer, T. J.; Baus, M.; Kurz, H. A Graphene Field-Effect Device. *IEEE Electron Device Lett.* **2007**, *28*, 282−284.

(11) Novoselov, K. Graphene: Mind the Gap. *Nat. Mater.* **2007**, *6*, 720−721.

(12) Novoselov, K. S.; Falko, V. I.; Colombo, L.; Gellert, P. R.; Schwab, M. G.; Kim, P. A Roadmap for Graphene. *Nature* **2012**, *490*, 192−200.

(13) Son, Y.-W.; Cohen, M. L.; Louie, S. G. Energy Gaps in Graphene Nanoribbons. *Phys. Rev. Lett.* **2006**, *97*, 216803.

(14) Barone, V.; Hod, O.; Scuseria, G. E. Electronic Structure and Stability of Semiconducting Graphene Nanoribbons. *Nano Lett.* **2006**, *6*, 2748−2754.
(15) Plasser, F.; Pašalić, H.; Gerzabek, M. H.; Libisch, F.; Reiter, R.; Burgdörfer, J.; Müller, T.; Shepard, R.; Lischka, H. The Multiradical Character of One- and Two-Dimensional Graphene Nanoribbons. *Angew. Chem., Int. Ed.* **2013**, *52*, 2581−2584.
(16) Li, X. L.; Wang, X. R.; Zhang, L.; Lee, S. W.; Dai, H. J. Chemically Derived, Ultrasmooth Graphene Nanoribbon Semiconductors. *Science* **2008**, *319*, 1229−1232.
(17) Gyunea, F.; Katsnelson, M. I.; Geim, A. K. Energy Gaps and a Zero-Field Quantum Hall Effect in Graphene by Strain Engineering. *Nat. Phys.* **2010**, *6*, 30−33.
(18) Zhang, Y. B.; Tang, T. T.; Girit, C.; Zhao, H.; Martin, M. C.; Zettl, A.; Crommie, M. F.; Shen, Y. R.; Wang, F. Direct Observation of a Widely Tunable Bandgap in Bilayer Graphene. *Nature* **2009**, *459*, 820−823.
(19) Castro, E. V.; Novoselov, K. S.; Morozov, S. V.; Peres, N. M. R.; Dos Santos, J.; Nilsson, J.; Guinea, F.; Geim, A. K.; Neto, A. H. C. Biased Bilayer Graphene: Semiconductor with a Gap Tunable by the Electric Field Effect. *Phys. Rev. Lett.* **2007**, *99*, 216802.
(20) (a) Tang, Q.; Zhou, Z.; Chen, Z. Graphene-related Nanomaterials: Tuning Properties by Functionalization. *Nanoscale* **2013**, *5*, 4541−4583. (b) Jiang, D. E., Chen, Z., Eds. *Graphene Chemistry: Theoretical Perspectives*; John Wiley & Sons: New York, 2013.
(21) Elias, D. C.; Nair, R. R.; Mohiuddin, T. M. G.; Morozov, S. V.; Blake, P.; Halsall, M. P.; Ferrari, A. C.; Boukhvalov, D. W.; Katsnelson, M. I.; Geim, A. K.; Novoselov, K. S. Control of Graphene's Properties by Reversible Hydrogenation: Evidence for Graphane. *Science* **2009**, *323*, 610−613.
(22) Sluiter, M. H.; Kawazoe, Y. Cluster Expansion Method for Adsorption: Application to Hydrogen Chemisorption on Graphene. *Phys. Rev. B* **2003**, *68*, 085410.
(23) Sofo, J. O.; Chaudhari, A. S.; Barber, G. D. Graphane: A Two-Dimensional Hydrocarbon. *Phys. Rev. B* **2007**, *75*, 153401.
(24) Samarakoon, D. K.; Wang, X.-Q. Chair and Twist-Boat Membranes in Hydrogenated Graphene. *ACS Nano* **2010**, *4*, 4017−4022.
(25) Lebegue, S.; Klintenberg, M.; Eriksson, O.; Katsnelson, M. I. Accurate Electronic Band Gap of Pure and Functionalized Graphane from GW Calculations. *Phys. Rev. B* **2009**, *79*, 245117.
(26) Nair, R.; Ren, W.; Jalil, R.; Riaz, I.; Kravets, V.; Britnell, L.; Blake, P.; Schedin, F.; Mayorov, A. S.; Yuan, S.; et al. Fluorographene: A Two-Dimensional Counterpart of Teflon. *Small* **2010**, *6*, 2877−2884.
(27) (a) Samarakoon, D. K.; Chen, Z. F.; Nicolas, C.; Wang, X. Q. Structural and Electronic Properties of Fluorographene. *Small* **2011**, *7*, 965−969. (b) Zbořil, R.; Karlický, F.; Bourlinos, A. B.; Steriotis, T. A.; Stubos, A. K.; Georgakilas, V.; Safárová, K.; Jancík, D.; Trapalis, C.; Otyepka, M. Graphene Fluoride: A Stable Stoichiometric Graphene Derivative and its Chemical Conversion to Graphene. *Small* **2010**, *6*, 2885−2891. (c) Karlický, F.; Zbořil, R.; Otyepka, M. Band Gaps and Structural Properties of Graphene Halides and Their Derivates: A Hybrid Functional Study with Localized Orbital Basis Sets. *J. Chem. Phys.* **2012**, *137*, 034709. (d) Karlický, F.; Datta, K. K. R.; Otyepka, M.; Zbořil, R. Halogenated Graphenes: Rapidly Growing Family of Graphene Derivatives. *ACS Nano* **2013**, *7*, 6434−6464. (e) Karlický, F.; Otyepka, M. Band Gaps and Optical Spectra of Chlorographene, Fluorographene and Graphane from G0W0, GW0 and GW Calculations on Top of PBE and HSE06 Orbitals. *J. Chem. Theory Comput.* **2013**, *9*, 4155−4164.
(28) Leenaerts, O.; Peelaers, H.; Hernández-Nieves, A. D.; Partoens, B.; Peeters, F. M. First Principles Investigation of Graphene Fluoride and Graphane. *Phys. Rev. B* **2010**, *82*, 195436.
(29) Li, Y.; Li, F.; Chen, Z. Graphane/Fluorographene Bilayer: Considerable C−H···F−C Hydrogen Bonding and Effective Band Structure Engineering. *J. Am. Chem. Soc.* **2012**, *134*, 11269−11275.
(30) Robinson, J. T.; Burgess, J. S.; Junkermeier, C. E.; Badescu, S. C.; Reinecke, T. L.; Perkins, F. K.; Zalautdniov, M. K.; Baldwin, J. W.; Culbertson, J. C.; Sheehan, P. E.; et al. Properties of Fluorinated Graphene Films. *Nano Lett.* **2010**, *10*, 3001−3005.
(31) Lee, W. -K.; Robinson, J. T.; Gunlycke, D.; Stine, R. R.; Tamanaha, C. R.; King, W. P.; Sheehan, P. E. Chemically Isolated Graphene Nanoribbons Reversibly Formed In Fluorographene Using Polymer Nanowire Masks. *Nano Lett.* **2011**, *11*, 5461−5464.
(32) Lee, W. H.; Suk, J. W.; Chou, H.; Lee, J.; Hao, Y.; Wu, Y.; Piner, R.; Akinwande, D.; Kim, K. S.; Ruoff, R. S. Selective-Area Fluorination of Graphene With Fluoropolymer and Laser Irradiation. *Nano Lett.* **2012**, *12*, 2374−2378.
(33) Ribas, M. A.; Singh, A. K.; Sorokin, P. B.; Yakobson, B. I. Patterning Nanoroads and Qauntum Dots on Fluorinated Graphene. *Nano Res.* **2011**, *4*, 143−152.
(34) Sahin, H.; Topsakal, M.; Ciraci, S. Structure of Fluorinated Graphene and Their Signatures. *Phys. Rev. B* **2011**, *83*, 115432.
(35) Wei, W.; Jacob, T. Electronic and Optical Properties of Fluorinated Graphene: A Many Body Perturbation Theory Study. *Phys. Rev. B* **2013**, *87*, 115431.
(36) Popov, I. V.; Li, Y.; Chen, Z.; Boldyrev, A. I. Benzation of Graphene upon Addition of Monovaleent Chemical Species. *Phys. Chem. Chem. Phys.* **2013**, *15*, 6842−6848.
(37) Fokin, A. A.; Gerbig, D.; Schreiner, P. R. $\sigma/\sigma$- and $\pi/\pi$-Interactions Are Equally Important: Multilayered Graphanes. *J. Am. Chem. Soc.* **2011**, *133*, 20036−20039.
(38) Janowski, T.; Pulay, P. A Benchmark Comparison of $\sigma/\sigma$ and $\pi/\pi$ Dispersion: The Dimers of Naphthalene and Decalin, and Coronene and Perhydrocoronene. *J. Am. Chem. Soc.* **2012**, *134*, 17520−17525.
(39) Li, Y.; Chen, Z. XH/$\pi$ (X = C, Si) Interactions in Graphene and Silicene: Weak in Strength, Strong in Tuning Band Structure. *J. Phys. Chem. Lett.* **2013**, *4*, 269−275.
(40) Guan, J.; Chen, W.; Li, Y.; Yu, G.; Shi, Z.; Huang, X.; Sun, C.; Chen, Z. Graphene Nanoribbons: An Effective Approach to Achieve a Spin Gapless Semiconductor-Half-Metal Transition in Zigzag Graphene Nanoribbons: Attaching A Floating Induced Dipole Field via $\pi$-$\pi$ Interactions. *Adv. Funct. Mater.* **2013**, *23*, 1507−1518.
(41) Tang, Q.; Zhou, Z.; Shen, P.; Chen, Z. Band Gap Engineering of BN Sheets by Interlayer Dihydrogen Bonding and Electric Field Control. *ChemPhysChem* **2013**, *14*, 1787−1792.
(42) Zhang, Z.; Guo, W.; Yakobson, B. I. Self-Modulated Band Gap in Boron Nitride Nanoribbons and Hydrogenated Sheets. *Nanoscale* **2013**, *5*, 6381−6387.
(43) Kresse, G.; Hafner, J. Ab Initio Molecular Dynamics for Liquid Metals. *Phys. Rev. B* **1993**, *47*, 558−561.
(44) (a) Blöchl, P. E. Projector Augmented-Wave Method. *Phys. Rev. B* **1994**, *50*, 17953−17979. (b) Kresse, G.; Joubert, D. From Ultrasoft Pseudopotentials to the Projector Augmented-Wave Method. *Phys. Rev. B* **1999**, *59*, 1758−1775.
(45) Perdew, J. P.; Burke, L.; Ernzerhof, M. Heneralized Gradient Approximation Made Simple. *Phys. Rev. Lett.* **1996**, *77*, 3865−3868.
(46) (a) Bettinger, H. F.; Kudin, K. N.; Scuseria, G. E. Structural Models of Fluorine-Graphite Intercalation Compounds from Density Functional Theory. *J. Phys. Chem. A* **2004**, *108*, 3016−3018. (b) Sato, Y.; Itoh, K.; Hagiwara, R.; Fukunaga, T.; Ito, Y. On the So-Called "Semi-Ionic" C-F Bond Character in Fluorine-GIC. *Carbon* **2004**, *42*, 3243−3249. (c) Claves, D. Spectroscopic Study of Fluorinated Carbon Nanostructures. *New J. Chem.* **2011**, *35*, 2477−2482.
(47) Reckien, W.; Jantzko, F.; Peintinger, M.; Bredow, T. Implementation of Empirical Dispersion Corrections to Density Functional Theory for Periodic Systems. *J. Comput. Chem.* **2012**, *33*, 2023−2031.
(48) (a) Moellmann, J.; Grimme, S. Importance of London Dispersion Effects for the Packing of Molecular Crystals: A Case Study for Intramolecular Stacking in a Bis-thiophene Derivative. *Phys. Chem. Chem. Phys.* **2010**, *12*, 8500−8504. (b) Ehrlich, S.; Moellmann, J.; Reckien, W.; Bredow, T.; Grimme, S. System-Dependent Dispersion Coefficients for the DFT-D3 Treatment of Adsorption Processes on Ionic Surfaces. *ChemPhysChem* **2011**, *12*, 3414−3420.

(49) Popov, I. A.; Li, Y.; Chen, Z.; Boldyrev, A. I. Benzation of Graphene upon Addition of Monovalent Chemical Species. *Phys. Chem. Chem. Phys.* **2013**, *15*, 6842−6848.
(50) Popov, I. A.; Boldyrev, A. I. Deciphering Chemical Bonding in a $BC_3$ Honeycomb Epitaxial Sheet. *J. Phys. Chem. C* **2012**, *116*, 3147−3152.
(51) (a) Heyd, J.; Scuseria, G. E.; Ernzerhof, M. Hybrid Functionals Based on a Screened Coulomb Potential. *J. Chem. Phys.* **2003**, *118*, 8207−8215. (b) Heyd, J.; Scuseria, G. E.; Ernzerhof, M. Erratum: Hybrid Functionals Based on a Screened Coulomb Potential. *J. Chem. Phys.* **2006**, *124*, 219906.
(52) For a review, see: Barone, V.; Hod, O.; Peralta, J. E.; Scuseria, G. E. Accurate Prediction of the Electronic Properties of Low-Dimensional Graphene Derivatives Using a Screened Hybrid Density Functional. *Acc. Chem. Res.* **2011**, *44*, 269−279.
(53) Wu, F.; Liu, Y.; Yu, G.; Shen, D.; Wang, Y.; Kan, E. Visible-Light-Absorption in Graphitic C3N4 Bilayer: Enhanced by Interlayer Coupling. *J. Phys. Chem. Lett.* **2012**, *3*, 3330−3334.
(54) Liu, Q.; Li, L.; Li, Y.; Gao, Z.; Chen, Z.; Lu, J. Tuning Electronic Structure of Bilayer $MoS_2$ by Vertical Electric Field: A First-Principle Investigation. *J. Phys. Chem. C* **2012**, *116*, 21556−21562.
(55) Zhang, Y. B.; Tang, T. T.; Girit, C.; Zhao, H.; Martin, M. C.; Zettl, A.; Crommie, M. F.; Shen, Y. R.; Wang, F. Direct Observation of a Widely Tunable Bandgap in Bilayer Graphene. *Nature* **2009**, *459*, 820−823.
(56) Lui, C. H.; Li, Z. Q.; Mak, K. F.; Capppeluti, E.; Heinz, T. F. Observation of an Electrically Tunable Band Gap in Trilayer Graphene. *Nat. Phys.* **2011**, *7*, 944−947.
(57) Geim, A. K.; Grigorieva, I. V. Van der Waals Heterostrucutres. *Nature* **2013**, *499*, 419−425.
(58) Haberer, D.; Guusca, C. E.; Wang, Y.; Sachdev, H.; Fedorov, A. V.; Farjam, M.; Jafari, S. A.; Vyalikh, D. V.; Usachov, D.; Liu, X. J.; et al. A. Evidence for A New Two-Dimensional C4H-Type Polymer Based on Hydrogenated Graphene. *Adv. Mater.* **2011**, *23*, 4497−4503.
(59) Li, Y.; Chen, Z. Patterned Partially Hydrogenated Graphene ($C_4H$) and Its One-Dimensional Analogues: A Computational Study. *J. Phys. Chem. C* **2012**, *116*, 4526−4534.
(60) Wu, J.; Xie, L.; Li, Y.; Wang, H.; Ouyang, Y.; Guo, J.; Dai, H. Controlled Chlorine Plasma Reacion for Noninvasive Graphene Doping. *J. Am. Chem. Soc.* **2011**, *133*, 19668−19671.